BEAM DYNAMICS IN MBA LATTICES WITH DIFFERENT CHROMATICITY CORRECTION SCHEMES *

L. Hoummi†, J. Resta Lopez and C. P. Welsch, University of Liverpool, Liverpool, UK and Cockcroft Institute, Daresbury, UK
A. Loulergue, R. Nagaoka, Synchrotron SOLEIL, Saint-Aubin, France

Abstract

Ultra-low emittance lattices are being studied for the future upgrade of the SOLEIL 2.75 GeV storage ring. The candidate baseline lattice is inspired by the ESRF-EBS type MBA lattice, introducing a $-I$ transformation to compensate the nonlinear impact of sextupoles thanks to the lattice symmetry and tight control of the betatron phase advance between sextupoles. Whilst its performance is under study, other types of lattices are being developed for SOLEIL: in particular, the so-called High-Order Achromat (HOA) lattice. Though the $-I$ scheme provides a large on-momentum transverse dynamic aperture in 4D, its off-momentum performance is limited. Further studies in 6D reveal intrinsic off-momentum transverse oscillations, which are considered to result from of a nonlinear increase of the path length. The effect of the inhomogeneous sextupole distribution in the $-I$ scheme shall be presented and compared with the HOA lattice under study.

INTRODUCTION

Towards the 4th generation of storage ring-based light sources, several ultra-low emittance lattices are considered to increase the brilliance of the photon sources. Due to being an upgrade, both circumference and energy are fixed for the existing machines: low emittance thus is obtained by MBA cells and strong focusing, leading to small dispersion and large natural chromaticity whose correction must now be integrated as a part of the lattice design.

Two chromaticity correction schemes are considered for the SOLEIL upgrade. The baseline lattice [1] uses the $-I$ transformation, setting a $((2k+1)\pi, n\pi)$ phase advance between two sextupoles (with k, n integers) for kick cancellation and optimised on-momentum acceptance, along with dispersion bumps at the location of the sextupoles for their increased efficiency and for global chromaticity correction. By contrast, local chromaticity correction is the aim of the so-called HOA lattice [2], built in several identical small cells, where phase advance is chosen to cancel geometric resonances over the MBA cell. Table 1 gathers the main characteristics of both lattices.

Despite its large on-momentum acceptance, the baseline lattice which is based upon the $-I$ transformation principle, presents a reduced effective dynamic aperture, as shown in Fig.1 when the synchrotron motion is taken into account in the tracking [1]: a strong coupling between the longitudinal and the transverse planes makes a particle go off-energy each turn – by increased path length, and falls out of the off-momentum acceptance. Such an effect is not explicitly seen in the HOA lattice.

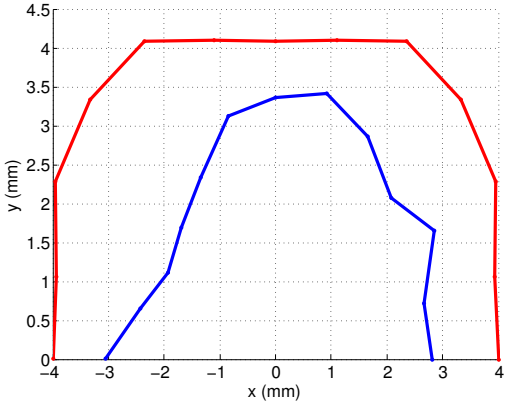

Figure 1: Transverse on-momentum dynamic aperture of a $-I$ cell, with natural chromaticities. In red, the lattice without RF, in blue, RF system added, with a voltage of 1.1 MV.

To understand this effect, and in order to reduce it, the path lengthening due to large amplitude betatron motions is studied in both lattices. The concerned effect depends on the chromaticity (ξ_x, ξ_y) in both planes [3]:

$$\Delta C = -2\pi(J_x\xi_x + J_y\xi_y), \quad (1)$$

where J_x and J_y are the horizontal and vertical action variables, respectively. The path length of both schemes is de-

Table 1: Lattices Characteristics

Chromatic correction scheme	$-I$	HOA
Energy	2.75 GeV	2.75 GeV
Symmetry	20	20
Tunes (ν_x, ν_y)	(55.2, 18.2)	(65.6, 24.6)
Natural emittance ϵ_x (pm rad)	72	77
Momentum compaction factor α_C	1.47E-4	1.09E-4
Energy spread	8.6E-4	7.8E-4

* This research was supported by SOLEIL and Cockcroft Institute core Grant No. ST/G008248/1.
† lina.hoummi@synchrotron-soleil.fr

rived using the 6D tracking modules available in Accelerator Toolbox and averaged over the input phase, after one turn to avoid any lost particle.

Figure 2 compares the tracked path length of each lattice with the theoretical path length in Eq. (1) at a corrected chromaticity $(\xi_x, \xi_y) = (1, 1)$. As no path lengthening is expected at small betatron amplitudes when the chromaticity is fully corrected, the $-I$ scheme exhibits a clear deviation from the expectation. The aim of this study is to analytically pursue the tracked averaged path length, for the low emittance lattices.

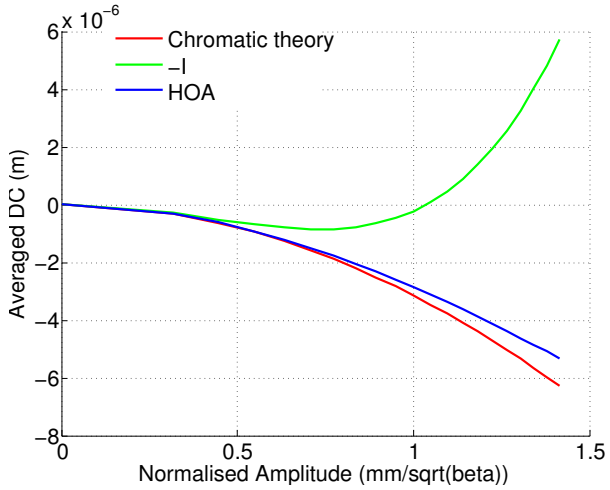

Figure 2: Path lengthening effect observed in the $-I$ (in green) lattice, for a corrected chromaticity (1, 1). The path length averaged over the input phase, follows a rule different from the known chromatic dependence in Eq. (1) (in red). The effect is less prominent in the HOA lattice (in blue).

FIRST-ORDER PERTURBATION THEORY

To understand this phenomenon, this paper refers to the canonical perturbation method used by M. Takao in [3], developed to recover the usual path lengthening formula in Eq. (1), by treating sextupoles as a perturbation to derive an averaged distorted transverse trajectory. The method is extended to first order in perturbation in the angular contribution in ΔC, $\langle x'^2 \rangle$. The perturbed Hamiltonian considered is:

$$H = \frac{p_x^2 + p_y^2}{2} + \frac{1}{2}(k_x^2 + g_0)x^2 - \frac{1}{2}g_0 y^2 + \frac{g_1}{3!}(x^3 - 3xy^2) + \frac{1}{2}k_x x(p_x^2 + p_y^2), \tag{2}$$

where where $p_{x,y}$ are the transverse beam momentum components, k_x is the horizontal curvature, g_0 and g_1 the quadrupole and sextupole strengths respectively. For the sake of ease in calculations, the following part is limited to the horizontal plane.

Averaged horizontal trajectory $\langle x \rangle$ Using the canonical perturbation theory described in [4], the distortion of the averaged trajectory coordinates (x, x') can be derived according to dipolar and sextupolar gradients.

$$\begin{aligned}
\langle x(s) \rangle_{\phi_x} = &- \frac{J_x\sqrt{\beta_x}}{4\sin(\pi\nu_x)} \int_s^{s+C} ds' \sqrt{\beta_x} \\
&\times (g_1\beta_x + k_x\gamma_x)\cos\left(\overline{\psi_x}(s', s)\right) \\
&- \frac{J_y\sqrt{\beta_x}}{4\sin(\pi\nu_x)} \int_s^{s+C} ds' \sqrt{\beta_x} \\
&\times (-g_1\beta_y + k_x\gamma_y)\cos\left(\overline{\psi_x}(s', s)\right) \\
&- \frac{J_x\sqrt{\beta_x}}{2\sin(\pi\nu_x)} \int_s^{s+C} ds' k_x \beta_x^{-1/2} \alpha_x \\
&\times \left(\sin\left(\overline{\psi_x}(s', s)\right) + \alpha_x \cos\left(\overline{\psi_x}(s', s)\right)\right) \\
&+ \frac{J_x\sqrt{\beta_x}}{4\sin(\pi\nu_x)} \int_s^{s+C} ds' k_x \beta_x^{-1/2} \cos\left(\overline{\psi_x}(s', s)\right),
\end{aligned} \tag{3}$$

where (ϕ_x, J_x) are the action-angle coordinates, $\beta_{x,y}$, $\alpha_{x,y}$ and $\gamma_{x,y}$ the Twiss parameters, $\overline{\psi_x}(s', s) = \phi_x(s') - \phi_x(s) - \pi\nu_x$, and ν_x the tune. Figure 3 demonstrates the good coincidence between the tracked mean trajectory and the analytical calculations.

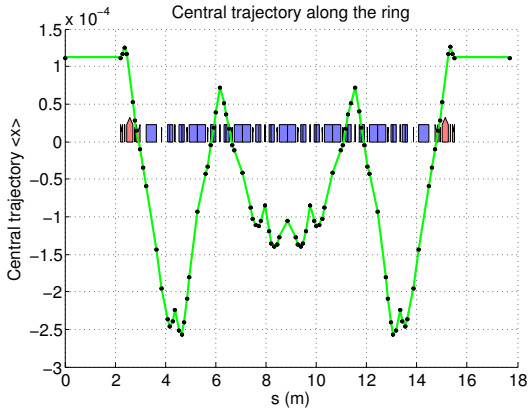

Figure 3: Averaged perturbed trajectory over one HOA cell: tracked (green lines) and calculated using Eq. (3) in black dots. The good match between the analytical calculation and the tracking ensures the convergence of the integrals over the ring.

Averaged horizontal angle $\langle x'^2 \rangle$ The second trajectory coordinate x' is derived from the Hamiltonian, considering that the perturbation is sufficient to differentiate the trajectory angle from the momentum: $x' = \frac{dx}{ds} = \frac{\partial H}{\partial p_x} = p_x(1 + k_x x)$. Following the same procedure as in [4], the contribution of the distorted trajectory angle in the path length is derived up to the first order in perturbation:

$$\begin{aligned}
\langle x'^2(s) \rangle_{\phi_x} = &\ J_x\gamma_x + k_x^2\alpha_x^2 J_x^2 + J_x^2 k_x^2 \frac{\beta_x\gamma_x}{2} \\
&+ 2k_x\alpha_x\sqrt{\frac{2J_x}{\beta_x}}\left(1 + \frac{\sqrt{J_x}}{2}\right)P_1 + k_x\sqrt{\frac{2J_x}{\beta_x}}\left(1 + \frac{\sqrt{J_x}}{2}\right)P_2,
\end{aligned} \tag{4}$$

where P_1 and P_2 are defined by:

$$
\begin{aligned}
P_1 = & \frac{J_x^{3/2}}{4\sqrt{2}\sin(\pi\nu_x)} \int_s^{s+C} ds' \sqrt{\beta_x} \\
& \times \left(g_1\beta_x + k_x(\gamma_x - \frac{1}{\beta_x}) \right) \\
& \times \left(\sin\left(\overline{\psi}(s',s)\right) - \alpha_x(s)\cos\left(\overline{\psi}(s',s)\right) \right) \\
& - \frac{J_x^{3/2}}{2\sqrt{2}\sin(\pi\nu_x)} \int_s^{s+C} ds' k_x \sqrt{\beta_x}\gamma_x\alpha_x \\
& \times (\alpha_x\alpha_x(s) + 1)\cos\left(\overline{\psi_x}(s',s)\right) \\
& - \frac{J_x^{3/2}}{2\sqrt{2}\sin(\pi\nu_x)} \int_s^{s+C} ds' k_x \sqrt{\beta_x}\gamma_x\alpha_x \\
& \times (\alpha_x - \alpha_x(s))\sin\left(\overline{\psi}(s',s)\right) \\
& + \frac{J_x^{1/2}J_y}{4\sqrt{2}\sin(\pi\nu_x)} \int_s^{s+C} ds' \sqrt{\beta_x}\left(-g_1\beta_y + k_x\gamma_y\right) \\
& \times \left(\sin\left(\overline{\psi}(s',s)\right) - \alpha_x(s)\cos\left(\overline{\psi}(s',s)\right) \right),
\end{aligned}
\tag{5}
$$

and

$$
\begin{aligned}
P_2 = & -\frac{J_x^{3/2}}{4\sqrt{2}\sin(\pi\nu_x)} \int_s^{s+C} ds' \sqrt{\beta_x}\beta_x(s)\gamma_x(s) \\
& \times \left(g_1\beta_x + k_x(\gamma_x - \frac{1}{\beta_x}) \right) \cos\left(\overline{\psi}(s',s)\right) \\
& - \frac{J_x^{1/2}J_y}{4\sqrt{2}\sin(\pi\nu_x)} \int_s^{s+C} ds' \sqrt{\beta_x}\beta_x(s)\gamma_x(s) \\
& \times \left(-g_1\beta_y + k_x\gamma_y\right)\cos\left(\overline{\psi}(s',s)\right) \\
& - \frac{J_x^{3/2}}{2\sqrt{2}\sin(\pi\nu_x)} \int_s^{s+C} ds' k_x\beta_x^{-1/2}\alpha_x\beta_x(s)\gamma_x(s) \\
& \times \left(\sin\left(\overline{\psi_x}(s',s)\right) + \alpha_x\cos\left(\overline{\psi_x}(s',s)\right) \right) \\
& - \frac{3J_x^{3/2}}{2\sqrt{2}\sin(3\pi\nu_x)} \int_s^{s+C} ds' k_x\beta_x^{-1/2}\alpha_x\beta_x(s)\gamma_x(s) \\
& \times \left(\sin\left(3\overline{\psi}(s',s)\right) - \alpha_x\cos\left(3\overline{\psi}(s',s)\right) \right) \\
& - \frac{3J_x^{3/2}}{\sqrt{2}\sin(3\pi\nu_x)} \int_s^{s+C} ds' k_x\beta_x^{-1/2}\alpha_x\alpha_x(s) \\
& \times \left(\cos\left(3\overline{\psi}(s',s)\right) - \alpha_x\sin\left(3\overline{\psi}(s',s)\right) \right) \\
& \frac{J_x^{3/2}}{4\sqrt{2}\sin(3\pi\nu_x)} \int_s^{s+C} ds' \sqrt{\beta_x}(g_1\beta_x - 3\frac{k_x}{\beta_x}) \\
& \times \left(2\alpha_x(s)\sin\left(3\overline{\psi}(s',s)\right) - \beta_x(s)\gamma_x(s)\cos\left(3\overline{\psi}(s',s)\right) \right).
\end{aligned}
\tag{6}
$$

HIGHER ORDER AVERAGED PATH LENGTHENING

Figure 4 compares the path length a function of the chromaticity Eq. (1), the 6D-tracked mean path length per turn and the application of the enlarged theory in the previous section. The tracked path length is obtained using 6D tracking over one turn, and averaging on the input phase, ensuring that the particles remain in a stability zone.

The analytical calculation of Eqs. (3) and (4) requires two levels of integration and convergence, obtained by slicing the lattice elements into 10, over the longitudinal coordinate s,

$$
\Delta C = \int_{s_0}^{s_0+C} ds \left(k_x\langle x\rangle + \frac{\langle x'^2\rangle}{2} \right). \tag{7}
$$

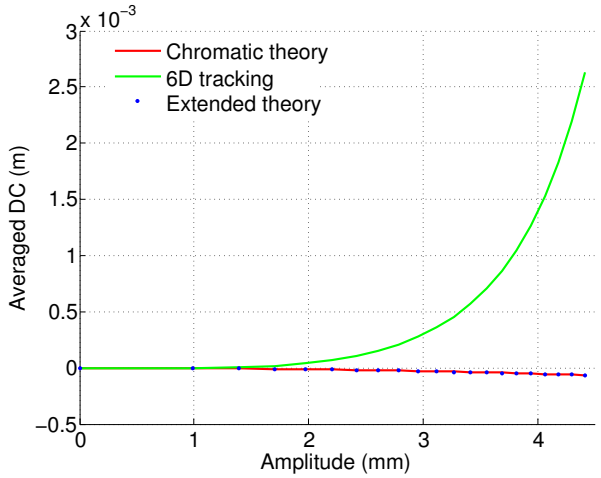

Figure 4: Averaged path lengthening considering the three described methods – linear formula (1) in red, 6D tracking of the $-I$ lattice in green and perturbated path length using Eqs. (3), (4)and (7), for corrected chromaticity (1, 1).

Higher-order terms will be required to describe the tracked path length of the low emittance lattices under study, as the first-order theory remains close to the general chromatic theory. The second order in perturbation, neglected in this contribution for the sake of simplicity, appears to be responsible for the path length effect in the low emittance lattices.

PERSPECTIVES

Considering that the first-order perturbation is not enough to describe the path lengthening observed in the $-I$ schemed lattice, including higher order perturbations should provide a better agreement with path length tracking results. Further studies including higher orders are ongoing and will be presented in future papers.

Provided that the extension of the present treatment achieves improved agreement, we shall attempt to reduce or even cancel the path lengthening effect observed in the $-I$ lattice. This optimisation may be done, either analytically or numerically using sextupoles, under the constraint of correcting the chromaticity, in order to restore its on-momentum performance.

REFERENCES

[1] A. Loulergue *et al.*, "Baseline Lattice for the Upgrade of SOLEIL", in *Proc. IPAC'18*, Vancouver, Canada, Apr.-May 2018, pp. 4726–4729. doi:10.18429/JACoW-IPAC2018-THPML034

[2] R. Nagaoka *et al.*, "Study of Higher-Order Achromat (HOA) Lattice as an Alternative Option for the SOLEIL Storage Ring Upgrade", presented at the 10th International Particle Accelerator Conf. (IPAC'19), Melbourne, Australia, May 2019, paper MOPRB005, this conference.

[3] M. Takao, "Impact of Betatron Motion on Path Lengthening and Momentum Aperture in a Storage Ring", in *Proc. EPAC'08*, Genoa, Italy, Jun. 2008, paper THPC072, pp. 3152–3154.

[4] M.Takao, Phys. Rev. E **72** (2005), 046502.